CHAPTER 20

Magnetic Tweezers in Cell Biology

Monica Tanase, Nicolas Biais, and Michael Sheetz

Department of Biological Sciences
Columbia University
New York, New York 10027

Abstract

We discuss herein the theory as well as some design considerations of magnetic tweezers. This method of generating force on magnetic particles bound to biological entities is shown to have a number of advantages over other techniques: forces are exerted in noncontact mode, they can be large in magnitude (order of 10 nanonewtons), and adjustable in direction, static or oscillatory. One apparatus built in our laboratory is described in detail, along with examples of experimental applications and results.

METHODS IN CELL BIOLOGY, VOL. 83

0091-679X/07 $35.00
DOI: 10.1016/S0091-679X(07)83020-2

I. Introduction

Form in biology, from cells to tissues and ultimately whole organisms, relies heavily on the sensing and generation of appropriate forces. The integrated response of the cell to forces controls cell growth and differentiation as well as extracellular matrix remodeling (Chen *et al.*, 2004; Chiquet *et al.*, 2003; Tamada *et al.*, 2004; Vogel and Sheetz, 2006). In the living organism, motile activity modulates the force over time and static forces are a rarity (Ito *et al.*, 2006; Maksym *et al.*, 2000; Meshel *et al.*, 2005; Murfee *et al.*, 2005). Thus, it is necessary to understand the dynamics of cellular force responses in order to understand cell growth and differentiation. An important example is the requirement for a substantive rather than overly soft substrate for normal cell growth since cancerous cells can often grow on soft agar (Discher *et al.*, 2005; Engler *et al.*, 2004; Georges and Janmey, 2005; Jiang *et al.*, 2006; Kostic and Sheetz, 2006). Changes in oncogenes are involved in enabling growth on soft agar (Giannone and Sheetz, 2006). We have relatively few tools for local modulation of forces at the nanonewton/micrometer levels that are typically observed in cells. Magnetic tweezers offer such capabilities and have many advantages over other force-generating systems.

A wide variety of methods have been developed to generate and measure cellular forces: micromechanical devices (Desprat *et al.*, 2005; Galbraith and Sheetz, 1997; Thoumine and Ott, 1997), fluid flow-based systems (Thomas *et al.*, 2004), atomic force microscopes (AFM) (Felix *et al.*, 2005; Lal and John, 1994), and optical (Sheetz, 1998) and magnetic tweezers (Bausch *et al.*, 1999; Crick and Hughes, 1950). They all have advantages as well as limitations in their applicability. This chapter focuses on magnetic tweezers. The term is generally used to describe an apparatus that applies a force to magnetic particles through magnetic field gradients. This method is noninvasive, as it allows micromanipulation without direct contact of particles bound to the biological entity under investigation: molecule, organelle, and cell. Such systems come in various designs and levels of complexity depending on the application pursued, and generally consist of an arrangement of permanent magnets or electromagnets mounted on an optical microscope stage. The aim of this chapter is to present the underlying principles of magnetic tweezers and to provide information to assist in optimally choosing and designing a system (see also complementary information in Chapter 19 by Lele *et al.*, this volume). The main performance parameters that need to be considered in building a magnetic force generation apparatus are:

1. Amplitude and direction of the force;
2. Timescale over which the force needs to be maintained or modulated—signal frequency;
3. Size of the assay—spatial range at which the force profile has the desired characteristics.

Advances in technologies and materials are continually expanding the available range of the parameters above, and thus the spectrum of capabilities of magnetic

tweezer systems. Amplitudes can vary from a few piconewtons (pN) (Strick *et al*., 1996) to tens of nanonewtons (nN) (Bausch *et al*., 1998; Strick *et al*., 1996). While many of the reported magnetic systems apply force in one direction only, a growing number of groups have been reporting designs that provide spatial flexibility in the direction of the force, including full 3D systems (Fisher *et al*., 2005). The timescale for force generation ranges from milliseconds (ms) to days, and frequencies can be as high as 5–10 kilohertz (kHz). The size of the assay can span from micrometers (Barbic *et al*., 2001; Jie *et al*., 2004) to centimeters (Haber and Wirtz, 2000). In designing a magnetic tweezers system, it is important to understand that these three categories of parameters are never independent of each other. Having an apparatus that operate in the high bandwidth of any of these parameters will significantly limit the range in the other two. Some of these limitations may be addressed partially by increasing the complexity of the system. Herein, we survey different possible magnetic tweezer assemblies and make note of some of the challenges involved in building systems that push the limits on the performance parameters.

II. Physics of Magnetic Tweezers

The working principle is that a magnetic particle placed in a magnetic field gradient will be subject to a force directed toward the source of the field. Two main components interact to create magnetic force: the profile of the external field and the magnetic properties of the particles used.

All materials are influenced to some degree by the presence of a magnetic field **B**, and their response is quantified by the magnetic moment $\boldsymbol{\mu}$ of the material. If this is nonzero, the material is said to be *magnetic*. The intensity and properties of the moment dictate the response of the material to externally applied fields. Most materials used for the construction of tweezer systems and the particles used to transduce the force to biological entities come in two major flavors: *paramagnetic*/*superparamagnetic* and *ferromagnetic*. *Paramagnetic* materials acquire a magnetic moment only when an external magnetic field is applied and are entirely nonmagnetic in zero field. *Ferromagnetic* materials are different in the sense that once exposed to a magnetic field, they become magnetized and will retain a certain fraction of their magnetization even after the field has been removed. Most commercially available beads (Fig. 1A) are *superparamagnetic*, a behavior similar to paramagnetism. Superparamagnetism occurs in materials containing ferromagnetic components (crystallites, nanoparticles) of dimensions small enough to cause the loss of their magnetic cohesion, that is their permanent magnetism, on removal of the external magnetic field. This is the case of most magnetic beads consisting of ferrite nanoparticles embedded in a spherical latex matrix. In contrast, ferromagnetic materials, such as nickel or cobalt nanowires (Fig. 1B), exhibit magnetic properties even when no external field is present (Fert and Piraux, 1999; Wernsdorfer *et al*., 1996). The magnetic moment of a ferromagnet depends not only on the value of the external field but on history of the magnetization of the

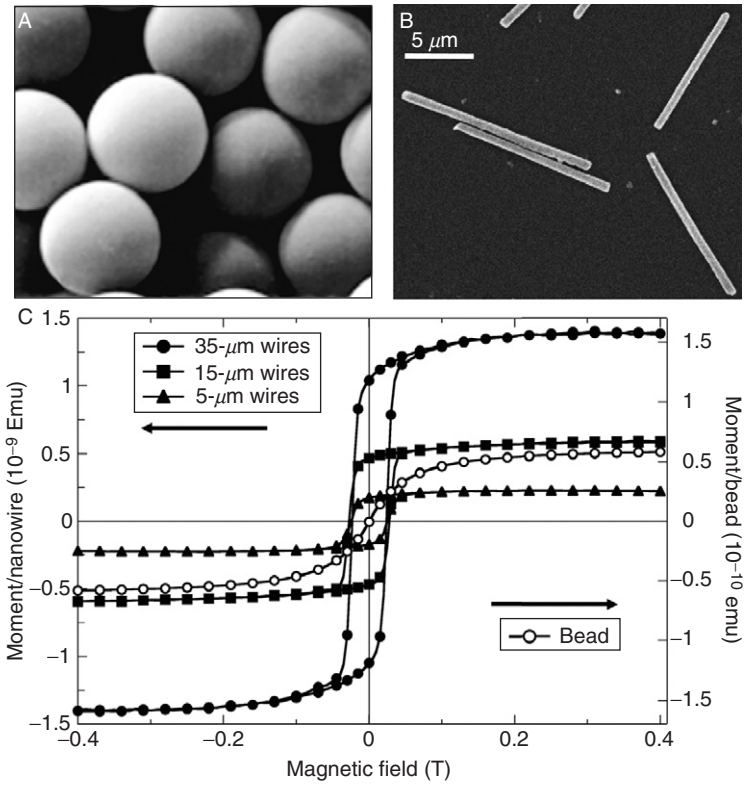

Fig. 1 Scanning electron microscope (SEM) images of (A) 4.5-μm paramagnetic beads (courtesy of Invitrogen Corporation, Dynal bead-based separations) and (B) electrodeposited nickel nanowires (Tanase *et al.*, 2005). (C) Hysteresis curves showing the dependence of the magnetic moment per particle $\boldsymbol{\mu}$ versus external magnetic field **B** for paramagnetic beads (1.5-μm diameter) and ferromagnetic nickel nanowires (100-nm diameter, 5-, 15- and 35-μm long); figure courtesy of Daniel H. Reich. Saturation occurs when the field is large enough to align all constituent magnetic moments, while remanence is the residual moment after the "relaxation" of alignment when the field is zero. Note that the hysteresis of the superparamagnetic beads is zero, as they exhibit no magnetic lag or memory effect. Emu on the *y*-axis stands for electromagnetic unit, the CGS unit for electromagnetic moment.

material, and this dependence is called *hysteresis* (Fig. 1C). The amount of magnetization that is retained when the driving field is removed is called *remanence*, and is an important parameter in the design of a magnetic tweezers system. We note here that it is possible to *demagnetize* a ferromagnetic material (such as the core of an electromagnet, see Section III.A) by rapidly cycling the external field between the positive and negative values necessary for saturation, and gradually dampening the amplitude of oscillations down to zero field. Such cycling will zero out the unwanted remanent magnetism of the ferromagnetic material.

A magnetic particle in a field is subject to mechanical forces of magnetic origin due to the interplay between its magnetic moment μ and the external field **B**.

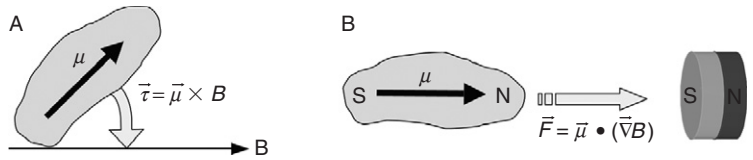

Fig. 2 Magnetic torque $\boldsymbol{\tau}$ and force **F**. Magnetic particles can be (A) rotated and (B) displaced via external magnetic fields.

A torque $\boldsymbol{\tau} = \boldsymbol{\mu} \times \mathbf{B}$ will tend to rotate and align the particle's moment with the external field, and in many cases the particle rotates itself to accommodate (Fig. 2A). If the field is not constant but presents a gradient $\nabla\mathbf{B}$, the particle is subject to a force proportional to the local field gradient $\mathbf{F} = (\boldsymbol{\mu}\cdot\nabla)\mathbf{B}$ directed toward the regions of higher magnetic field (Fig. 2B).

In summary, a magnetic particle will rotate to align its magnetic moment parallel to the magnetic field direction, and translate toward the regions of higher field. While magnetic particles can consequently be pulled in the direction of increasing fields, they can never be pushed away. If flexibility is required in the directionality of the force, multiple magnetic poles, as well as the use of nonpermanent field, need to be implemented in the system (de Vries *et al.*, 2005; Drndic *et al.*, 2001; Fisher *et al.*, 2005; Huang *et al.*, 2002).

III. Magnetic Field Considerations

We discuss here methods of generating magnetic fields and various aspects of the field gradient profile. Unless noted, the observations here refer to the field of a single magnetic pole. In the case of multiple poles, magnetic circuitry principles need to be considered.

A. Sources of Magnetic Field

In a magnetic tweezers apparatus, permanent magnets (Matthews *et al.*, 2004) or electromagnets can be used as sources of field. While a permanent magnet generates a static permanent field, electromagnets convert electrical currents into magnetic field and allow control of the field through control of the current.

Permanent magnets are the most accessible method for producing a magnetic field (Fig. 3A). When made of rare earth materials, they can generate fields as large as 0.8 T (for comparison, Earth's magnetic field is $\sim 0.5 \times 10^{-4}$ T). Their field is very steady but in order to modulate it the magnets need to be physically displaced—action that limits the time response of the system and can potentially add mechanical noise. In contrast, electromagnets typically generate fields that are orders of magnitude lower than those of equal or equivalent sized permanent magnets, but they have the great advantage that the amplitude of the magnetic field can be controllably and rapidly modulated. The simplest version of an

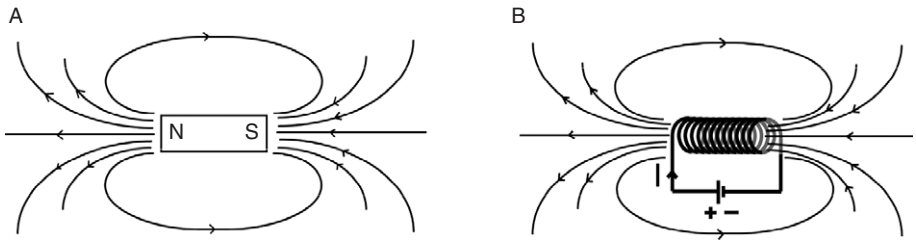

Fig. 3 Schematic of magnetic field profiles for (A) permanent magnet and (B) and an electromagnetic solenoid.

electromagnet is a coiled conductive wire. If multiple coils form a cylindrical geometry, the structure is called a *solenoid* (Fig. 3B). When electrical current runs through the wire, a magnetic field is established in the direction of the solenoid's axis. We note here that cylindrical permanent magnets and solenoids produce magnetic fields with similar profiles (Fig. 3), albeit different magnitudes.

The strength of the field produced by an electromagnet is set by the value of the current in the wire and the coil geometry. To amplify the magnetic field, a magnetic core can be positioned inside the solenoid. Cores are typically made from soft ferromagnetic materials with high saturation and low remanence. While such designs allow stronger local fields, they introduce another problem: the existence of a remnant magnetic field. Even when the current is turned off, the core remains magnetized to some extent, and therefore a remnant force is exerted on the targeted particle. As previously discussed, this effect can be reduced by running a cycle of demagnetization on the core or by using a more elaborate design with multiple coils. To produce large forces using an electromagnet, either large-diameter coils or high electrical currents are needed. The size of the solenoid (length and diameter) will be limited by the physical specifications of the apparatus and the ease of use. Large currents may generate heating in the coils, detrimental to the magnetic core and ultimately to the biological sample. To circumvent this problem, heat sinks or cooling systems are typically used (Haber and Wirtz, 2000).

B. Magnet Pole Design

While the amplitude of the field is important, it is the gradient of the magnetic field $\nabla\mathbf{B}$ that directly factors into the magnitude of the force. The gradient is the strongest close to the magnet, as the field drops in magnitude faster nearer the magnet than further away from it. A convenient rule of thumb in approximating the gradient one can obtain with a magnet is that most of the field will vanish within a distance that is roughly the size of the pole diameter. The size of the magnet is therefore directly coupled to the size of the experimental assay. If, for example, the force needs to be constant over an extended range such as the field of view of the microscope, then $\nabla\mathbf{B}$ needs to also be constant over the same area. This

can be obtained either by using a blunt large magnet that will generate a slowly decreasing magnetic field, that is small gradient, or by doing the experiment further away from any type of pole, in the region where the variance of the field tapers off. Elaborate systems with multiple poles can produce constant gradients but at the expense of the force amplitude. Generation of large forces require large field gradients. This is typically obtained by tapering off the magnet or the electromagnetic core at the pole on the sample side to concentrate the magnetic flux. At the same time, the specimen should be positioned close to the magnetic tip. A sharpened pole face gives a larger gradient and force. For example, if a magnet generates a 0.5-T field and the cross section is 1 cm, the average gradient near the magnet is on the order of 50 T/m and the force is $\mu_{\text{particle}} \times 50$ T/m. If the magnet is sharpened (e.g., magnetized sewing needle) such that the pole face is small, the gradient can be much larger but over a much smaller distance. The cross section could be made as small as 10 μm, and for a face field of 0.5 T the local magnetic gradient is on the order of 5×10^4 T/m. The force in this case would be three orders of magnitude larger than that with the blunt geometry, provided that the moment of the particles is the same.

While magnetic tweezers are force clamps by the nature of the interaction, they can be designed to serve as position clamps. Such a design cannot be passive as it requires active control of the position of the particle and entails at the very least a position feedback system (Gosse and Croquette, 2002). Overall, electromagnets offer more control on the spatial and temporal profile of the magnetic field generated but at the price of increasing the technical challenges.

IV. Magnetic Particle Selection

In order to apply a magnetic force to a biological sample, a magnetic particle needs to be bound to the sample. A variety of particles, typically superparamagnetic beads, are currently used for physical manipulation of cells and biomolecules (Hafeli *et al.*, 1997). For most of the magnetic tweezer applications, consistency in the magnetic and geometric characteristics of the particles is very important. A large selection of magnetic beads is available with very low standard deviations in both diameter and magnetic content (Bangs Laboratories Fishers, Indiana; Polysciences Inc., Warrington, Pennsylvania; Invitrogen Corporation, Carlsbad, California). The most common type of paramagnetic bead consists of a spherical latex matrix containing dispersed magnetic nanoparticles. As previously mentioned, the force scales with the magnetic moment of the particle and, consequently, to the volume of magnetic material present in the particle. The overall volume of the bead is not the only relevant factor for the magnitude of force; another determining factor is the magnetic content. For example, 1-μm-diameter Dynal beads (MyOne, Invitrogen Corporation, Carlsbad, California) have 34% magnetic content, while the 2.7-μm beads (M270, Invitrogen Corporation, Carlsbad, California) contain 20% ferrite material.

Another type of magnetic particles available from Polysciences, Inc., 1- to 2-μm-diameter BioMagPlus, has been specifically engineered for separation applications.

They consist of a solid ferrite core amounting to 90% magnetic content, and are coated with a thin latex layer. The resulting magnetic force per particle is larger than other types of beads of similar diameter. One other difference is that unlike the spherical beads, these are irregularly shaped in order to produce a greater surface area, 20–30 times that of a spherical particle of the same size (Polysciences, Inc., technical data sheet No. 618). While the greatly increased area results in greater molecular binding, the volume and therefore magnetic content are different from particle to particle, resulting in a large variance (~100%) in the magnetic force across the population. The advantage of using these beads with magnetic tweezers is that much larger forces can be applied through small particles, but the force calibration has very large error margins. However, if the accuracy of the force measurement is not important but high binding efficiency is, such particles are preferred.

Magnetic nanowires (Fig. 1B) constitute another class of nanostructures suitable for magnetic tweezer applications (Reich *et al.*, 2003; Tanase *et al.*, 2005). These are quasi-one-dimensional cylindrical structures with large aspect ratios, with diameters in the 1–1000 nm range and lengths from tens of nanometers to tens of micrometers. While there are various methods for fabricating nanowires, one particularly attractive approach is electrodeposition into nanoporous templates (Whitney *et al.*, 1993). Due to the fabrication process, the composition along the length of electrodeposited nanowires can be precisely modulated, which in turn enables precise control of the architecture of the magnetic properties (Blondel *et al.*, 1994; Chen *et al.*, 2003). In addition, by using ligands that bind selectively to different segments of a multicomponent wire, it is possible to introduce spatially modulated multiple functionalization in the wires (Bauer *et al.*, 2003; Tanase *et al.*, 2001). Also, their strong shape anisotropy gives rise to preferential direction of the magnetic moment and therefore new properties (Hultgren *et al.*, 2005). The unique features of magnetic nanowires greatly expand the range of functions performed by magnetic particles. These include:

- A large remnant magnetic moment offering the prospect of low-field manipulation, whereas larger fields are required for the beads to become magnetic enough to be effective;
- Large forces and torques that can be applied to cells and biomolecules; forces can be up to 1000 times larger than the forces on beads of comparable volumes;
- Larger surface area providing increased adhesion surface;
- Multifunctional surfaces, as multiple bioactive ligands can be selectively bound to the different segments of multicomponent nanowires.

Magnetic tweezers are also used for studies of the inside of living cells (Basarab *et al.*, 2003; Francois *et al.*, 1996; Marion *et al.*, 2005). In some cases, the magnetic beads or nanowires are too large and a different category of particles is needed. One option is the use of ferrofluids which are magnetic nanoparticles in aqueous suspensions. The ferrofluids can be loaded into the cells via endocytosis, allowing the study of the structure of cytoplasm and organelles in which the particles are

concentrated (Marion *et al.*, 2005; Valberg and Albertini, 1985; Wilhelm *et al.*, 2003).

One other factor that needs to be considered in choosing a suitable type of particle is whether fluorescence imaging is involved. As latex is an autofluorescent material, most of the magnetic beads on the market exhibit this effect. Examples of particles that are not autofluorescent are the irregularly shaped BioMagPlus and ferromagnetic nanowires.

As can be concluded, particles come in different sizes, shapes, surfaces, and optical and magnetic properties. Depending on the application intended, one or another type of particle may be more desirable, and the choice of use depends among others on the type of forces and torques needed as well as on the available surface chemistry.

V. Basic Solenoid Apparatus

In this section, we describe the design and construction of a magnetic tweezers apparatus currently used in our laboratory (Fig. 4), built to generate forces as large as 10 nN with frequencies from 0 to 1 kHz, values that match and exceed those found in tissues. One use of this system is the application of local forces at the position of interest on cells: lamellipodium, lamella, and perinuclear region, via magnetic beads attached to specific receptors on the cellular dorsal surface. The trajectory of the beads is the result of the interplay between the magnetic force and the force exerted by the cell on the bead. As the force applied on the cell via the beads can be modulated as desired within the system's specifications, the cellular response to a specific mechanostimulus can be investigated.

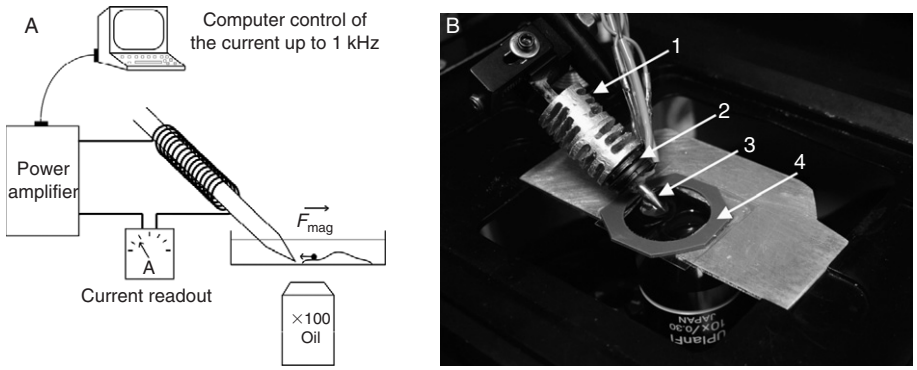

Fig. 4 (A) Schematic representation of the magnetic tweezers and imaging system. The current in the solenoid is controlled via computer through a power amplifier. (B) Electromagnetic system used in our laboratory, composed of (1) a heat-dissipating aluminium sheath, (2) three copper coils, (3) ferromagnetic core, and (4) the experimental chamber.

An electromagnet with a ferromagnetic core sharpened at the sample side was built to concentrate the magnetic field and allow generation of high-amplitude forces on micrometer-sized particles (Fig. 4A). The core of the electromagnet is 2.5 mm in diameter and is made of a soft magnetic alloy with very high saturation and low remanence (Hyperco50, The MuShield Company, Manchester, New Hampshire) in order to allow high magnetic flux without saturation at the tip, while minimizing the magnitude of the remnant fields inside the core after applying large currents. To further assure the repeatability of the measurement, a demagnetizing cycle is used to zero the field inside the core prior to each experiment. We note here one practical drawback of using magnetic materials with small-remnant field that they are not easily amenable to machining. Typically, magnetic materials with small remnant fields are quite brittle and great care must be taken to maintain an intact sharpened tip once the machining is completed.

A key component for this electromagnetic system is the current in the coils (fabricated in-house, 20 turns per coil, copper wire). In order to meet our system design needs, a power transconductance amplifier was generously provided by the Center for Computer Integrated Systems for Microscopy and Manipulation at University of North Carolina (Fisher *et al.*, 2005). This can independently supply three separate coils (Fig. 4A) with currents proportional to their input voltages. The drive amplifier is powered by the output of a National Instruments Acquisition Board, controlled through a LabVIEW designed computer user interface (Fig. 4B). This system permits the current in each coil to reach up to 5 A at frequencies up to 1 kHz. A three-axis micromanipulator allows tip positioning with submicron precision.

Another factor that can negatively influence the experiment is the heat generation due to the use of large currents. A significant increase in temperature would adversely affect the magnetic properties of the core and decrease the amplitude and gradient of the generated magnetic field. Additionally, if the heat transfer results in even a few degrees rise in the biological sample, the experimental results could be significantly affected. The easiest way to address the heating due to high currents is to introduce even the thinnest gap between the core and the coils to serve as a thermally insulating buffer, and to add aluminum heat sinks directly onto the core of the electromagnet. In our system, heat dissipation is adequate to prevent a temperature increase in the biological sample while producing high local field gradients. Currents up to 2 A can be maintained indefinitely without detectable heating of the coils. Higher currents may be used, but only intermittently in short pulses to allow time for heat dissipation.

VI. Force Calibration

The output of a *force calibration procedure* is a graph of the force versus the distance from the magnetic tip, and is a function of the magnetic particle used, the current in the coils, and in some cases the angle between the core axis and

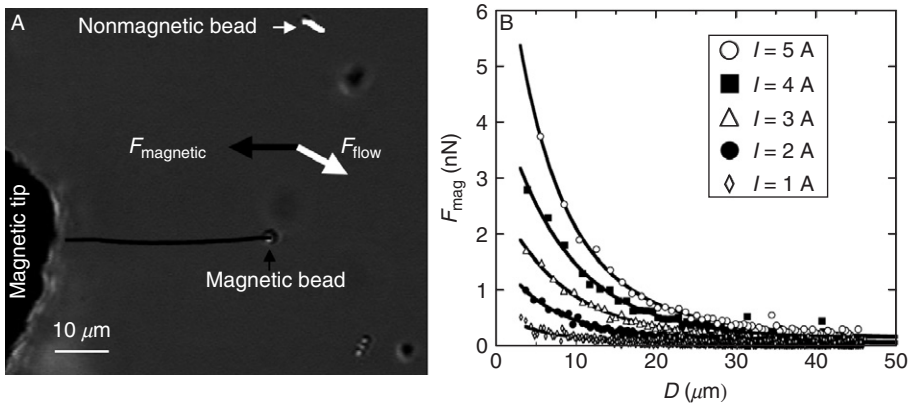

Fig. 5 Force calibration of magnetic tweezers. (A) Trajectories of a 2.7-μm magnetic bead (black trace) and a 1-μm polystyrene bead (white trace) suspended in 1000-cp standard viscosity oil. (B) Graph of force versus distance from the edge of the magnetic tip for coil currents of 1, 2, 3, 4, and 5 A.

the particle's position vector (Fig. 5B). Once this *force calibration curve* has been generated, it can be used to determine the value of the magnetic force on a bead attached to a biological entity, by recording its location relative to the magnetic tip.

It is theoretically possible to calculate the force exerted on a magnetic particle in a known field profile. However, inherent inaccuracies in the physical and geometrical properties of the system components make this approach rather impractical. It is common practice to determine the forces empirically, by tracking the displacement of the particles through stationary fluids of calibrated viscosity. An important dimensionless number in fluid dynamics is the Reynolds number, used for determining whether a flow is laminar or turbulent. It is defined as the ratio of inertial to viscous forces $Re = v_s \rho L/\eta$, where v_s is the mean fluid velocity, ρ is the fluid density, η is the dynamic fluid viscosity, and L is the characteristic particle length (particle diameter in the case of magnetic beads). For microparticles, Reynolds number is typically very small ($Re < 10^{-5}$), so viscous drag dominates over all other hydrodynamic effects and the flow is laminar (Lifshitz and Landau, 1959). In this regime, in response to an applied force F, a particle will move with terminal velocity $v = F/D$, where D is the appropriate drag coefficient. For a spherical particle, Stokes' law gives $D = 6\pi\eta r$, where r is the radius of the bead. In the case of nanowires, the drag coefficient for a cylinder has the same functional form as for a sphere, but r in this case is the effective radius and may be determined by approximating the wire as a prolate ellipsoid (Lamb, 1945). Consequently, by tracking the displacement of an unbound microparticle under magnetic force, the velocity versus position dependence can be obtained. The force can then be calculated as $F = 6\pi\eta r v$.

A. Calibration Sample Protocol

We found that the displacement of the magnetic beads under force induces motion of the viscous fluid surrounding them, and that after a certain period a concerted flow is established in the direction of the magnetic field gradient. In order to be able to use the described Stokes calibration, the drift of the fluid needs to be either avoided or taken into account. To monitor the displacement of the fluid itself, nonmagnetic beads are added into the fluid (Fig. 5A). These are nonresponsive to the magnetic force and are used as fluid flow markers. For optical identification, the two types of beads are chosen to be of different diameter, with the nonmagnetic beads smaller than the magnetic ones. The density of the magnetic beads is kept very low in order to delay the onset of fluid flow during calibration. The final density of beads in suspension depends on how well the beads are dispersed in the mix. On visual inspection, the optimum density of magnetic beads is such that they are spaced at least 20 diameters from each other, and the density of polystyrene beads is approximately three to four times larger. The volumes in the following procedure are to be used as a starting point and one should visually inspect the sample to determine the optimal dilution.

Calibration chamber: Small volume silicone chamber (9-mm diameter; 1-mm height; press-to-seal silicone isolators—Grace Bio-Labs, Inc., Bend, Oregon, Cat. No. JTR8R-1.0) fitted with cover glass bottom.

Materials: Magnetic carboxylate spheres (Dynal, M270), polystyrene beads (Bangs Laboratories, Fishers, Indiana, Cat. No. PS03N), calibrated viscosity silicone oil (dimethylpolysiloxane, Sigma-Aldrich, St. Louis, Missouri, Cat. No. DMPS1C-1000G), rare earth magnets (NdFeB discs, Amazing Magnets, Irvine, CA, Cat. No. D250C).

Stock solutions of both types of beads have to be homogenized prior to use, by gentle vortexing.

Silica beads

- Make a 1:10 dilution in milliQ water, briefly vortex.
- Add 5 μl of the diluted bead solution to 95 μl of milliQ water, centrifuge the beads down (4 min, 10,000 rpm) in a tabletop centrifuge, and carefully remove as much supernatant as possible.
- Add 1 ml of silicone oil and mix thoroughly. (Note: beads stored in aqueous suspensions are difficult to disperse in oils as they often close pack in micellar structures.)

Magnetic beads

- Make a 1:10 dilution of magnetic beads in milliQ water, briefly sonicate.
- Place 5 μl of the diluted magnetic bead solution into an Eppendorf tube (10^4 beads in the case of M270 beads from a stock concentration of 2×10^7 beads/ml).
- Using the magnet, collect all the beads onto one side of the water droplet, and with the magnet in place, use a small pipette tip to remove as much of the water supernatant as possible.

- Add 200 μl of oil suspension of silica beads, mix thoroughly with a 200-μl pipette tip to disperse and incorporate the magnetic beads.
- Place 65 μl of the resulting mixture in the calibration chamber.

Potential problems

1. Bead aggregation: carboxylate beads in water do not mix well into oil, micelles form. Remove as much water as possible, mix thoroughly.
2. If the suspension of polystyrene and magnetic beads has incorporated air bubbles, place the tube in a vacuum chamber until clear.
3. Glass binding: some of the beads are near the glass substrate and their mobility is reduced due to glass binding; these beads should not be used for calibration. Note that beads in suspension settle; therefore, gentle mixing with a pipette tip to resuspend them is required after 1–2 h (settling time is proportional to the oil viscosity).

B. Calibration Procedure

Place the calibration chamber on the optical microscope, search for a suitable single magnetic bead in the neighborhood of a few polystyrene ones, all in the same plane of focus. Insert the magnetic tip into the silicone oil to the depth of the chosen beads, as judged under the microscope. For calibration, a magnetic bead is considered "suitable" if it is:

- not surrounded by water
- positioned at least 20 diameters away from another magnetic bead
- more than 5 diameters away from the glass bottom of the chamber, as judged using the focusing mechanism of the microscope

Allow few minutes for the solution to settle and the beads to become mostly still. Start the image acquisition and apply the desired magnetic force. Allow the bead to reach the magnetic tip. Zero the current in the coil and demagnetize the core. Wait until the flow has ceased, then look for the next bead. Repeat as many times as needed at different angles from the needle for statistical significance.

C. Direction of Magnetic Force

As the solenoid and the core are not horizontal, the magnetic force will not be horizontal either. To minimize the vertical component, we flatten the bottom of the magnetic tip [method also reported in Bausch *et al.* (1998)]. With this geometry the force on the beads is mostly horizontal, with a slight angle that increases in the proximity of the tip. We estimate that 3 to 5 μm away from the tip, the force vector forms a 10° angle with the horizontal plane. In this case, the vertical component of the force accounts for 15% of the total force giving a proportional

15% error in the calibration curve, which is within the system's overall errors. We note here that a number of magnetic tweezer systems have been designed to generate vertical force (Assi *et al.*, 2002; Gosse and Croquette, 2002). The force versus distance calibration procedure often involves correlation of the diffraction rings of an ascending bead (Gosse and Croquette, 2002).

The force produced by any magnetized cylinder such as the tweezers core varies as a function of the angle between the bead's position vector and the axial direction of the cylindrical magnet core. The greatest force at equal distance from the tip is in the axial direction, and the force decreases as the angle increases. However, the dependence on the angle of approach becomes insignificant in the proximity of the tip, at a length scale on the order of the radius of the magnetic tip. In our case, the radius was on the order of 50 μm, and no difference was observed in the force profile across 50 μm from the tip, for angles up to 45° from the core axis.

D. Bead-Tracking System

Optical images are acquired by either a high-resolution CCD camera or through a video acquisition system allowing 30 frames/sec. The location of the bead is determined frame-by-frame by a position-tracking algorithm based on a cross-correlation image analysis (Gelles *et al.*, 1988) giving subpixel resolution (0.1–0.2 pixel error). The code is implemented as a plug-in in ImageJ (NIH, available in public domain). The subsequent data interpretation and modeling is done in IGOR Pro (WaveMetrics Inc., Lake Oswego, Oregon).

E. Data Interpretation

In an image sequence of a magnetic bead approaching the tip under magnetic forces, multiple targets should be tracked for accuracy in addition to the calibrating bead. The motion of at least one nonmagnetic bead reveals the displacement of the fluid itself and serves as a background displacement vector. The position of the magnetic tip should also be tracked, as even a few micrometers of positional drift would result in an erroneous calibration of the force, especially in the regions closest to the tip.

The error in the calibration of forces includes standard deviations for the bead's magnetic content and diameter, actual temperature of the oil (optical imaging can locally heat the observed volume of fluid and locally change the viscosity of these standardized oils—dimethylpolysiloxane), unaccounted vertical component of magnetic forces, and errors in position tracking. We estimate that the overall error is less than 15%.

VII. Experimental Procedures

In the *in vivo* cellular host environments such as the ECM, tissues, or organs, oscillations occur due to the contractile activity of cells or cyclical activities of the host organism. The magnetic tweezers assay can mimic the manner by which extracellular forces are applied to cells in tissues by allowing well-controlled generation of pulsatory mechanical signals of large magnitudes. We detail here example applications where constant and oscillatory forces were applied to beads bound to mammalian cells, and we describe the data interpretation along with cautionary notes on potential problems and sources of errors.

Spherical 2.7-μm-diameter Dynal beads (M270, Polysciences, Inc.) were functionalized with a pentamer of fibronectin's integrin-binding domain FNIII7–10 (Jiang *et al*., 2003) according to the protocol included in the product data sheet (Dynabeads, M270, carboxylic acid technical sheet, Rev. No. 002). The beads were placed on laminin-coated glass substrates and the cells were subsequently allowed to spread. In a typical "spreading assay," when the protruding edge of a cell makes contact with a bead, integrins are ligated and activated and initial adhesive contacts form. The beads are therefore bound to the cell membrane and displaced by the rearward actin flow in a radial trajectory toward the nucleus. The velocity of the beads depends on a number of factors, including the level of motile cell activity, the type of ligands present on the beads, and the region of the cell the beads traverse. Bead displacement is, for example, faster on the lamellipodium, slower and less directional in the perinuclear region, and fairly constant in speed and direction across the lamella. Beads functionalized with FN pentamer traverse the lamellar region of a spreading cell at an average speed of 70 nm/sec (Jiang *et al*., 2003).

The magnetic tweezers allow the application of localized stress to the dorsal surface of the cells via beads bound to specific receptors. The assay enables the study of cellular response to spatially localized mechanostimulus through observation of the trajectory resulting from the interplay between the magnetic and cellular forces. We describe here one representative case where large magnetic force was used (0.5–0.6 nN) (Fig. 6). Once the bead was observed to engage in rearward motion, a constant level of force was applied in the direction opposite to the cell force (Fig. 6A). The graph in Fig. 6B shows the distance between the bead and the cell edge D_{edge} versus time (upper panel), as well as the corresponding magnitude of the applied magnetic force (lower panel). As can be seen in Fig. 6A when the bead is moving away from the edge of the cell and toward the nucleus, D_{edge} increases indicating that $F_{cell} > F_{mag}$. When the magnetic force prevails over the cell force, the bead moves toward the edge of the cell and D_{edge} decreases. When the force is initially applied, a rapid displacement of the bead occurs in the direction of the magnetic tip (markers 2 to 3 in Fig. 6B and C) and can be attributed partly to rolling and partly to a viscoelastic response of the cell. This is followed typically by fluctuations in the bead's velocity and direction of movement even when the level

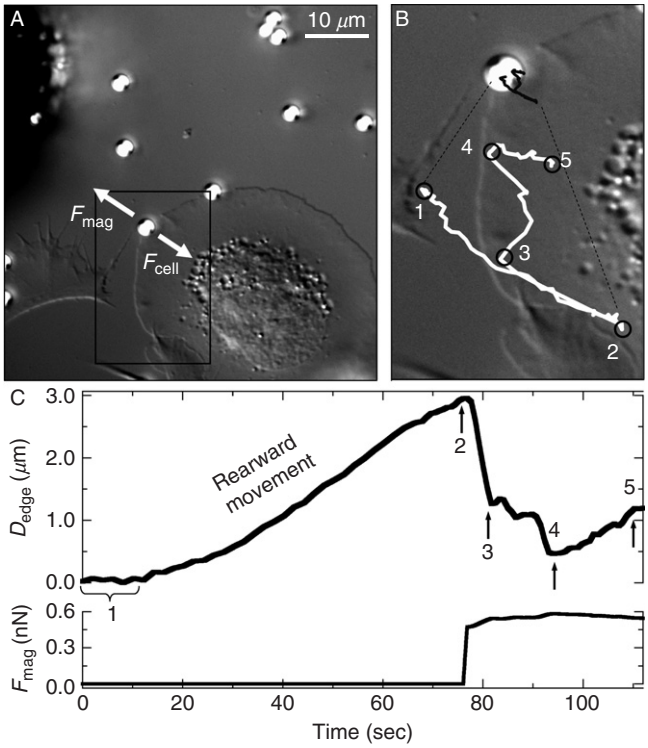

Fig. 6 Constant force assay. (A) Magnetic tweezers (tip located at top left corner) exert force on 2.7-μm magnetic beads bound to a spreading fibroblast. (B) Close-up of the rectangular region marked in panel (A). The actual trajectory of the bead is marked in black, and shown enlarged as the white trace. Prior to application of force, the rearward flow of actin displaces the bead from the cell edge (position 1–2), toward the nucleus. When the external force is applied (position 2), the bead moves under the competing action of the two forces, cellular and magnetic. (C) D_{edge} versus time graph. In response to application of force, the cell responds by pulling in a contractile manner (positive- and negative-rearward velocities) and reinforces the cytoskeletal adhesion to the stress site (position 3–4). The end of the adaptive period is marked by the recovery of the bead's constant rate of displacement (position 4–5).

of force is sustained (e.g., by doing experiments in a far region from the tip where the variation of the force with position is slow), then by the restoration of constant rearward bead velocity (markers 4 to 5). Since the magnetic force is constant, the variations in bead velocity (seen between markers 3 to 4) indicate fluctuations in the cell force and/or breakage of the association. As the cell adapts to the local stress, it generates pulsatory traction forces at the site of the mechanical signal, that is the bead. This is reminiscent of the periodic lamellipodial contractions in spreading and migrating cells (Dobereiner *et al.*, 2005; Dubin-Thaler *et al.*, 2004; Giannone

and Sheetz, 2006; Giannone *et al*., 2004). By using the magnetic tweezers assay, controlled activation of mechanosignaling can be induced at levels of force (up to about 10 nN) and with large numbers of beads not possible with other systems. In contrast, the maximum force of the optical tweezers is only about 100 pN and nanometer precision tracking systems are needed to keep the force constant for a single bead.

Cells show adaptive strengthening in response to large modulated stresses (Matthews *et al*., 2006). Application of oscillatory local stimuli via the magnetic tweezers permits observation of these changes through the tracking of the beads' displacements. In the experiment illustrated in Fig. 7, a square wave force of 1.4- to 1.6-nN amplitude and 4-sec period (2-sec pulse width) is applied to a bead bound to the lamellipodium of a spreading cell. After the initial forward thrust with the force application, the bead shows oscillation movement with a fairly constant amplitude for a few cycles, then the amplitude begins to decrease indicating

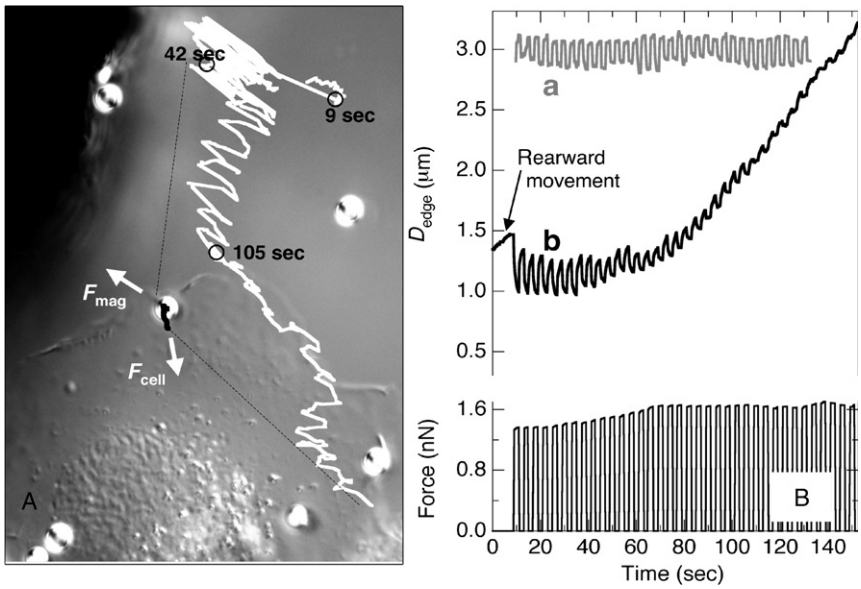

Fig. 7 Modulated force assay. (A) Oscillatory force is applied to a 2.7-μm bead bound to the lamellipodium of a spreading fibroblast. The trajectory of the bead is shown in black for the actual size, and white for the close-up. For 9 sec preceding the force application, the bead undergoes rearward movement. The amplitude of oscillations begins decreasing at the 42-sec time point, and rearward movement is restored at 105 sec. (B) Upper panel: D_{edge} versus time graph for the bead on cell (black trace b), and one bead on the substrate (gray trace a) for comparison. Lower panel: magnetic force versus time. The amplitude of oscillation can be seen to decrease and the velocity of the bead (curve slope) to increase to values comparable to that before stress.

reinforcement of the integrin–cytoskeleton adhesion. Only afterward (96 sec after application of force) the cell reengages the bead in the rearward movement while maintaining a small amplitude of bead oscillation. Such an assay can be used on cells expressing fluorescent adhesion proteins to further elucidate the dynamics of cellular response to mechanical stress. We note here that modulated force waveforms have been extensively used to study the rheology of the cytoplasm, the actomyosin gel, organelles (Basarab *et al.*, 2003; Fabry *et al.*, 2001; Hu *et al.*, 2004; Keller *et al.*, 2001; Mack *et al.*, 2004; Matthews *et al.*, 2006; Valberg and Albertini, 1985; Wilhelm *et al.*, 2003; Ziemann *et al.*, 1994), and whole-cell assays (Thoumine and Ott, 1997).

In the experiments described here, the following targets were tracked in the image analysis stage:

- The bead under observation.
- Beads on the substrate that are bound to the glass through FN-laminin linkage. These beads roll under magnetic force and return to their initial position when the force is turned off, unless breakages occur in the protein structure anchoring them to the substrate. Their motion under force constitutes a qualitative *in situ* control of the magnetic force.
- The location of magnetic tip.
- Fiduciary structures on the cover glass to enable the tracking of substrate drift.

Observation of the motion of all these targets allows one to check and account for mechanical coupling, drift, noise, and system integrity. It also serves to verify the repeatability of the experimental conditions. The pattern of bead motion on the substrate should, for example, be similar if the experimental conditions are not modified. Observed changes may indicate changes in the calibrated force, substrate, or bead coating.

In this chapter, we have discussed a variety of magnetic tweezer designs and different types of applications of magnetic particles to the study of mechanotransduction and cell mechanical properties. Because of the different goals in each application, the optimal magnetic particles and optimal magnetic field configuration will differ. The particular application that we have discussed is to produce high forces on beads specifically bound to matrix receptors. For those experiments, a single sharpened magnetic probe is optimal. Important considerations in the design include thermal isolation of the tip from the coils to prevent sample heating and the choice of the beads. Although the measurement of absolute force is relatively inaccurate, at these large forces relative values provide useful measures of the mechanisms controlling force. Further, *in vivo* there are large oscillations in the level of mechanical forces that are applied to the cells. Thus, the ability to produce high and variable forces so rapidly is important for probing the mechanisms of cell mechanical functions.

References

Assi, F., Jenks, R., Yang, J., Love, C., and Prentiss, M. (2002). Massively parallel adhesion and reactivity measurements using simple and inexpensive magnetic tweezers. *J. Appl. Phys.* **92,** 5584–5586.

Barbic, M., Mock, J. J., Gray, A. P., and Schultz, S. (2001). Scanning probe electromagnetic tweezers. *Appl. Phys. Lett.* **79,** 1897–1899.

Basarab, G. H., Karoly, J., Peter, B., Ferenc, I. T., and Gabor, F. (2003). Magnetic tweezers for intracellular applications. *Rev. Sci. Instrum.* **74,** 4158–4163.

Bauer, L. A., Reich, D. H., and Meyer, G. J. (2003). Selective functionalization of two-component magnetic nanowires. *Langmuir* **19,** 7043–7048.

Bausch, A. R., Moller, W., and Sackmann, E. (1999). Measurement of local viscoelasticity and forces in living cells by magnetic tweezers. *Biophys. J.* **76,** 573–579.

Bausch, A. R., Ziemann, F., Boulbitch, A. A., Jacobson, K., and Sackmann, E. (1998). Local measurements of viscoelastic parameters of adherent cell surfaces by magnetic bead microrheometry. *Biophys. J.* **75,** 2038–2049.

Blondel, A., Meier, J. P., Doudin, B., and Ansermet, J.-P. (1994). Giant magnetoresistance of nanowires of multilayers. *App. Phys. Lett.* **65,** 3019–3021.

Chen, C. S., Tan, J., and Tien, J. (2004). Mechanotransduction at cell–matrix and cell–cell contacts. *Annu. Rev. Biomed. Eng.* **6,** 275–302.

Chen, M., Sun, L., Bonevich, J. E., Reich, D. H., Chien, C. L., and Searson, P. C. (2003). Tuning the response of magnetic suspensions. *Appl. Phys. Lett.* **82,** 3310–3312.

Chiquet, M., Renedo, A. S., Huber, F., and Fluck, M. (2003). How do fibroblasts translate mechanical signals into changes in extracellular matrix production? *Matrix Biol.* **22,** 73–80.

Crick, F. H. C., and Hughes, A. F. W. (1950). The physical properties of cytoplasm: A study by means of the magnetic particle method Part I. Experimental. *Exp. Cell Res.* **1,** 37–80.

de Vries, A. H. B., Krenn, B. E., van Driel, R., and Kanger, J. S. (2005). Micro magnetic tweezers for nanomanipulation inside live cells. *Biophys. J.* **88,** 2137–2144.

Desprat, N., Richert, A., Simeon, J., and Asnacios, A. (2005). Creep function of a single living cell. *Biophys. J.* **88,** 2224–2233.

Discher, D. E., Janmey, P., and Wang, Y. L. (2005). Tissue cells feel and respond to the stiffness of their substrate. *Science* **310,** 1139–1143.

Dobereiner, H. G., Dubin-Thaler, B. J., Giannone, G., and Sheetz, M. P. (2005). Force sensing and generation in cell phases: Analyses of complex functions. *J. Appl. Physiol.* **98,** 1542–1546.

Drndic, M., Lee, C. S., and Westervelt, R. M. (2001). Three-dimensional microelectromagnet traps for neutral and charged particles. *Phys. Rev. B* **63,** 085321-1–085321-4.

Dubin-Thaler, B. J., Giannone, G., Dobereiner, H. G., and Sheetz, M. P. (2004). Nanometer analysis of cell spreading on matrix-coated surfaces reveals two distinct cell states and STEPs. *Biophys. J.* **86,** 1794–1806.

Engler, A. J., Griffin, M. A., Sen, S., Bonnemann, C. G., Sweeney, H. L., and Discher, D. E. (2004). Myotubes differentiate optimally on substrates with tissue-like stiffness: Pathological implications for soft or stiff microenvironments. *J. Cell Biol.* **166,** 877–887.

Fabry, B., Maksym, G. N., Shore, S. A., Moore, P. E., Panettieri, R. A., Jr., Butler, J. P., and Fredberg, J. J. (2001). Signal transduction in smooth muscle: Selected contribution: Time course and heterogeneity of contractile responses in cultured human airway smooth muscle cells. *J. Appl. Physiol.* **91,** 986–994.

Felix, R., Pere, R.-C., Nuria, G., Ramon, F., Mar, R., and Daniel, N. (2005). Probing mechanical properties of living cells by atomic force microscopy with blunted pyramidal cantilever tips. *Phys. Rev. E* **72,** 021914-1–021914-10.

Fert, A., and Piraux, L. (1999). Magnetic nanowires. *J. Mag. Mag. Mater.* **200,** 338–358.

Fisher, J. K., Cummings, J. R., Desai, K. V., Vicci, L., Wilde, B., Keller, K., Weigle, C., Bishop, G., Taylor, R. M., II, Davis, C. W., Boucher, R. C., O'Brien, T. E., *et al.* (2005). Three-dimensional

force microscope: A nanometric optical tracking and magnetic manipulation system for the biomedical sciences. *Rev. Sci. Instrum.* **76,** 053711-1–053711-11.

Francois, A., Bernard, Y., Andrew, P., and Stanislas, L. (1996). A magnetic manipulator for studying local rheology and micromechanical properties of biological systems. *Rev. Sci. Instrum.* **67,** 818–827.

Galbraith, C. G., and Sheetz, M. P. (1997). A micromachined device provides a new bend on fibroblast traction forces. *Proc. Natl. Acad. Sci. USA* **94,** 9114–9118.

Gelles, J., Schnapp, B. J., and Sheetz, M. P. (1988). Tracking kinesin-driven movements with nanometre-scale precision. *Nature* **331,** 450–453.

Georges, P. C., and Janmey, P. A. (2005). Cell type-specific response to growth on soft materials. *J. Appl. Physiol.* **98,** 1547–1553.

Giannone, G., Dubin-Thaler, B. J., Dobereiner, H. G., Kieffer, N., Bresnick, A. R., and Sheetz, M. P. (2004). Periodic lamellipodial contractions correlate with rearward actin waves. *Cell* **116,** 431–443.

Giannone, G., and Sheetz, M. P. (2006). Substrate rigidity and force define form through tyrosine phosphatase and kinase pathways. *Trends Cell Biol.* **16,** 213–223.

Gosse, C., and Croquette, V. (2002). Magnetic tweezers: Micromanipulation and force measurement at the molecular level. *Biophys. J.* **82,** 3314–3329.

Haber, C., and Wirtz, D. (2000). Magnetic tweezers for DNA micromanipulation. *Rev. Sci. Instrum.* **71,** 4561–4570.

Hafeli, U., Schutt, W., and Joachim, T. (1997). "Scientific and Clinical Applications of Magnetic Carriers." Plenum, New York.

Hu, S., Eberhard, L., Chen, J., Love, J. C., Butler, J. P., Fredberg, J. J., Whitesides, G. M., and Wang, N. (2004). Mechanical anisotropy of adherent cells probed by a three-dimensional magnetic twisting device. *Am. J. Physiol. Cell Physiol.* **287,** C1184–C1191.

Huang, H., Dong, C. Y., Kwon, H.-S., Sutin, J. D., Kamm, R. D., and So, P. T. C. (2002). Three-dimensional cellular deformation analysis with a two-photon magnetic manipulator workstation. *Biophys. J.* **82,** 2211–2223.

Hultgren, A., Tanase, M., Felton, E. J., Bhadriraju, K., Salem, A. K., Chen, C. S., and Reich, D. H. (2005). Optimization of yield in magnetic cell separations using nickel nanowires of different lengths. *Biotechnol. Prog.* **21,** 509–515.

Ito, S., Majumdar, A., Kume, H., Shimokata, K., Naruse, K., Lutchen, K. R., Stamenovic, D., and Suki, B. (2006). Viscoelastic and dynamic nonlinear properties of airway smooth muscle tissue: Roles of mechanical force and the cytoskeleton. *Am. J. Physiol. Lung Cell. Mol. Physiol.* **290,** L1227–L1237.

Jiang, G., Giannone, G., Critchley, D. R., Fukumoto, E., and Sheetz, M. P. (2003). Two-piconewton slip bond between fibronectin and the cytoskeleton depends on talin. *Nature* **424,** 334–337.

Jiang, G., Huang, A. H., Cai, Y., Tanase, M., and Sheetz, M. P. (2006). Rigidity sensing at the leading edge through alphavbeta3 integrins and RPTPalpha. *Biophys. J.* **90,** 1804–1809.

Jie, Y., Dunja, S., and John, F. M. (2004). Near-field-magnetic-tweezer manipulation of single DNA molecules. *Phys. Rev. E* **70,** 011905-1–011905-5.

Keller, M., Schilling, J., and Sackmann, E. (2001). Oscillatory magnetic bead rheometer for complex fluid microrheometry. *Rev. Sci. Instrum.* **72,** 3626–3634.

Kostic, A., and Sheetz, M. P. (2006). Fibronectin rigidity sensing through Fyn and p130Cas recruitment at the leading edge. *Mol. Biol. Cell.* **17,** 2684–2695.

Lal, R., and John, S. A. (1994). Biological applications of atomic force microscopy. *Am. J. Physiol. Cell Physiol.* **266,** C1–C21.

Lamb, H. (1945). "Hydrodynamics," 6th edn. Dover, New York.

Lifshitz, E., and Landau, L. (1959). "Fluid Mechanics." Pergamon Press, Oxford.

Mack, P. J., Kaazempur-Mofrad, M. R., Karcher, H., Lee, R. T., and Kamm, R. D. (2004). Force-induced focal adhesion translocation: Effects of force amplitude and frequency. *Am. J. Physiol. Cell Physiol.* **287,** C954–C962.

Maksym, G. N., Fabry, B., Butler, J. P., Navajas, D., Tschumperlin, D. J., Laporte, J. D., and Fredberg, J. J. (2000). Mechanical properties of cultured human airway smooth muscle cells from 0.05 to 0.4 Hz. *J. Appl. Physiol.* **89,** 1619–1632.

Marion, S., Guillen, N., Bacri, J.-C., and Wilhelm, C. (2005). Acto-myosin cytoskeleton dependent viscosity and shear-thinning behavior of the amoeba cytoplasm. *Eur. Biophys. J.* **34,** 262–272.

Matthews, B. D., Overby, D. R., Alenghat, F. J., Karavitis, J., Numaguchi, Y., Allen, P. G., and Ingber, D. E. (2004). Mechanical properties of individual focal adhesions probed with a magnetic microneedle. *Biochem. Biophys. Res. Commun.* **313,** 758–764.

Matthews, B. D., Overby, D. R., Mannix, R., and Ingber, D. E. (2006). Cellular adaptation to mechanical stress: Role of integrins, Rho, cytoskeletal tension and mechanosensitive ion channels. *J. Cell Sci.* **119,** 508–518.

Meshel, A. S., Wei, Q., Adelstein, R. S., and Sheetz, M. P. (2005). Basic mechanism of three-dimensional collagen fibre transport by fibroblasts. *Nat. Cell Biol.* **7,** 157–164.

Murfee, W. L., Hammett, L. A., Evans, C., Xie, L., Squire, M., Rubin, C., Judex, S., and Skalak, T. C. (2005). High-frequency, low-magnitude vibrations suppress the number of blood vessels per muscle fiber in mouse soleus muscle. *J. Appl. Physiol.* **98,** 2376–2380.

Reich, D. H., Tanase, M., Hultgren, A., Bauer, L. A., Chen, C. S., and Meyer, G. J. (2003). Biological applications of multifunctional magnetic nanowires (invited). *J. Appl. Phys.* **93,** 7275–7280.

Sheetz, M. P. (1998).''Laser Tweezers in Cell Biology,'' Vol. 55. Academic Press, San Diego, California.

Strick, T. R., Allemand, J.-F., Bensimon, D., Bensimon, A., and Croquette, V. (1996). The elasticity of a single supercoiled DNA molecule. *Science* **271,** 1835–1837.

Tamada, M., Sheetz, M. P., and Sawada, Y. (2004). Activation of a signaling cascade by cytoskeleton stretch. *Dev. Cell* **7,** 709–718.

Tanase, M., Bauer, L. A., Hultgren, A., Silevitch, D. M., Sun, L., Reich, D. H., Searson, P. C., and Meyer, G. J. (2001). Magnetic alignment of fluorescent nanowires. *Nano Lett.* **1,** 155–158.

Tanase, M., Felton, E. J., Gray, D. S., Hultgren, A., Chen, C. S., and Reich, D. H. (2005). Assembly of multicellular constructs and microarrays of cells using magnetic nanowires. *Lab Chip* **5,** 598–605.

Thomas, W. E., Nilsson, L. M., Forero, M., Sokurenko, E. V., and Vogel, V. (2004). Shear-dependent 'stick-and-roll' adhesion of type 1 fimbriated Escherichia coli. *Mol. Microbiol.* **53,** 1545–1557.

Thoumine, O., and Ott, A. (1997). Time scale dependent viscoelastic and contractile regimes in fibroblasts probed by microplate manipulation. *J. Cell Sci.* **110,** 2109–2116.

Valberg, P. A., and Albertini, D. F. (1985). Cytoplasmic motions, rheology, and structure probed by a novel magnetic particle method. *J. Cell Biol.* **101,** 130–140.

Vogel, V., and Sheetz, M. (2006). Local force and geometry sensing regulate cell functions. *Nat. Rev. Mol. Cell Biol.* **7,** 265–275.

Wernsdorfer, W., Doudin, B., Mailly, D., Hasselbach, K., Benoit, A., Meier, J., Ansermet, J. P., and Barbara, B. (1996). Nucleation of magnetization reversal in individual nanosized nickel wires. *Phys. Rev. Lett.* **77,** 1873.

Whitney, T. M., Jiang, J. S., Searson, P. C., and Chien, C. L. (1993). Fabrication and magnetic properties of arrays of metallic nanowires. *Science* **261,** 1316–1319.

Wilhelm, C., Cebers, A., Bacri, J. C., and Gazeau, F. (2003). Deformation of intracellular endosomes under a magnetic field. *Eur. Biophys. J.* **32,** 655–660.

Ziemann, F., Radler, J., and Sackmann, E. (1994). Local measurements of viscoelastic moduli of entangled actin networks using an oscillating magnetic bead micro-rheometer. *Biophys. J.* **66,** 2210–2216.